Last Glacial Maximum ice sheet impacts on North Atlantic climate variability: The importance of the sea ice lid

Guido Vettoretti[1] and W. Richard Peltier[1]

Received 25 October 2013; revised 3 December 2013; accepted 3 December 2013; published 23 December 2013.

[1] Last Glacial Maximum (LGM) ICE-5G (VM2), ICE-6G (VM5a), and Paleoclimate Modelling Intercomparison Project Phase 3 ice sheet reconstructions are employed in high-resolution coupled climate model simulations to investigate the changes they induce in North Atlantic climate variability. An initial ICE-5G (VM2) experiment develops a rapid increase of sea ice extent once a thermal threshold is exceeded in this multimillennial simulation. Subpolar sea ice concentration and thickness are found to be strongly impacted by topographically induced downstream thermal effects from the Laurentide Ice Sheet in each of the reconstructions. However, in the two additional LGM perturbation experiments, the modeled changes in sea ice area are sufficiently similar to the LGM ICE-5G (VM2) experiment to lead to an equilibrium Atlantic Meridional Overturning Circulation strength that is also reduced by the same ~40% from preindustrial even though we find significant variation among the models in the deep convection regions of the subpolar glacial North Atlantic. Model-predicted sea ice concentrations in this critical region exceed those based upon multiproxy reconstructions, and we trace these significant differences to the intensity of the interannual variability of sea ice cover predictions. **Citation:** Vettoretti, G., and W. R. Peltier (2013), Last Glacial Maximum ice sheet impacts on North Atlantic climate variability: The importance of the sea ice lid, *Geophys. Res. Lett.*, *40*, 6378–6383, doi:10.1002/2013GL058486.

1. Introduction

[2] Several studies have led their authors to the conclusion that the North Atlantic Deep Water (NADW) cell was in a sluggish state at the Last Glacial Maximum (LGM), between 26,000 and 21,000 years ago [*Peltier and Fairbanks*, 2006], with Antarctic Bottom Water intruding much farther into the North Atlantic abyssal ocean than it does under modern conditions [*Oppo and Curry*, 2012]. Reductions in Atlantic Meridional Overturning Circulation (AMOC) strength have been inferred on the basis of changes in Pa/Th ratios [*McManus et al*., 2004], reductions in nutrient concentration in North Atlantic Intermediate Water [*Boyle and Leach*, 1995], reductions in North Atlantic primary productivity [*Radi and de Vernal*, 2008], and variations in the LGM Atlantic zonal density contrast inferred from oxygen isotopes in benthic foraminifera [*Lynch-Stieglitz et al*., 2007].

[3] The second phase of the Paleoclimate Modelling Intercomparison Project (PMIP2) included model predictions of both stronger and weaker LGM AMOC strength with respect to modern control simulations [*Weber et al*., 2007; *Kageyama et al*., 2013]. PMIP3 also includes many experiments in which the Atlantic Thermohaline Circulation is predicted to be stronger than modern by up to 12 sverdrups (Sv) [e.g., *Brady et al*., 2013]. *Oka et al*. [2012] have suggested that there could exist a thermal threshold governing the extent of deep convection in the northern North Atlantic and the strength of the AMOC by perturbing the surface forcing in an ocean-sea ice model. In their study the strength of the AMOC was found to be dependent on the strength of the cooling and/or wind stress forcing in the North Atlantic in each of the forced ocean model simulations analyzed. Their results were invoked to suggest an explanation for the differences in equilibrium AMOC strength obtained in PMIP2 intercomparisons [e.g., *Otto-Bliesner et al*., 2007]. However, it remains unclear whether a similar thermal threshold effect would arise in a fully coupled free-running simulation of LGM climate. It has also been suggested that differences in LGM AMOC strength may also be related to physical processes in the Southern Ocean or to ocean-specific subgrid-scale parameterizations [e.g., *Mashayek et al*., 2013].

[4] Using a coupled atmosphere-ocean general circulation model, we investigate the downstream impacts that different land ice sheet reconstructions are expected to have on the state of the LGM North Atlantic and its connection to sea ice dynamics and the strength of the AMOC.

2. Model and Experimental Design

2.1. Model

[5] We have employed a slightly modified version of the fully coupled National Center for Atmospheric Research Community Climate System Model Version 3 (CCSM3) with atmosphere (T85L26: ~1.4° × 1.4°), land (~1.4° × 1.4°), ocean (~1° × 1°: L40), and sea ice (~1° × 1°) components [*Collins et al*., 2006]. The model components and modifications to the boundary conditions for the preindustrial control and LGM simulations are described in section 3 and supporting information where Table S1 provides a summary of the boundary and initial conditions. The resolution employed in our analyses is significantly higher than in any previous CCSM3-based reconstruction of LGM climate.

2.2. Ice Sheet Forcing

[6] The three different ice sheet boundary conditions employed to simulate LGM climate in the current study are those for the ICE-5G (VM2) model that was stipulated for PMIP2, the ICE-6G_A reconstruction [*Peltier*, 1994, 2004; *Argus and Peltier*, 2010], and the blended ice sheet product

Additional information may be found in the online version of this article.

[1]Department of Physics, University of Toronto, Toronto, Ontario, Canada.

Corresponding author: G. Vettoretti, Department of Physics, University of Toronto, 60 St. George St., Toronto, ON M5R 3B9, Canada. (g.vettoretti@utoronto.ca)

0094-8276/13/10.1002/2013GL058486

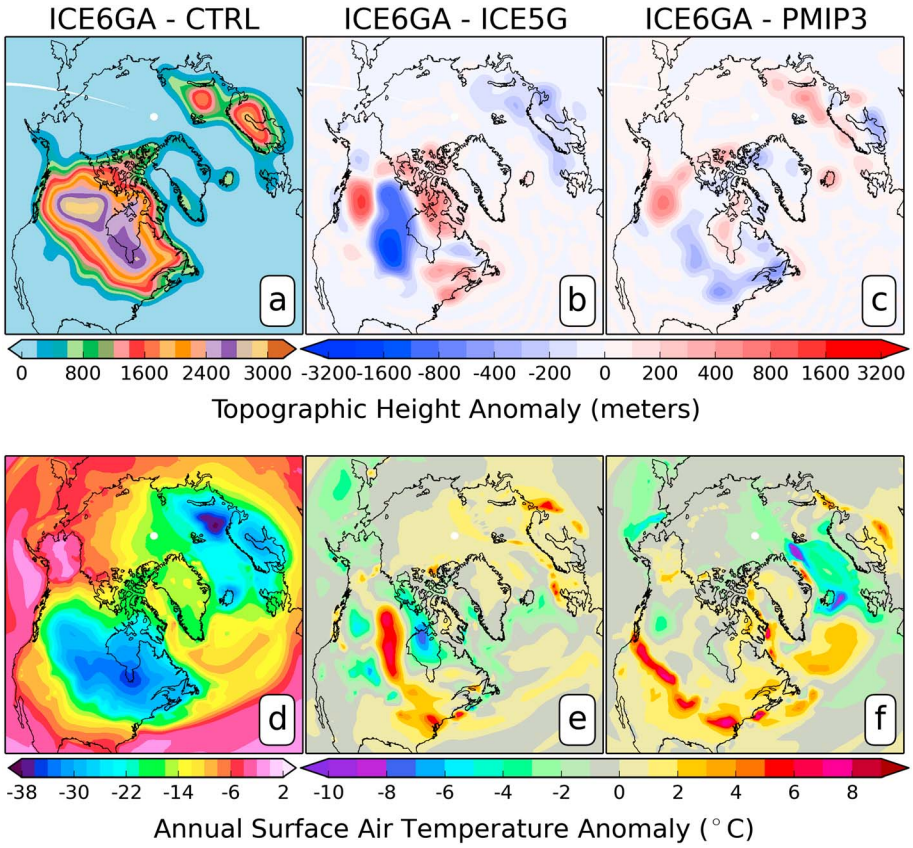

Figure 1. Differences in the Laurentide Ice Sheet topography (meters) with respect to sea level between (a) LGM ICE-6G_A and modern, (b) ICE-6G_A and ICE-5G, and (c) ICE-6G_A and PMIP3. (d–f) Same as in Figures 1a–1c but for surface air temperature (°C).

mandated for use in PMIP3. The blended product consists of a (as yet unpublished in detail) mixture of three different ice sheet reconstructions, namely ICE-6G_A (see *Argus and Peltier* [2010] for the data on the basis of which ICE-6G_A has been constructed), Meltwater routing and Ocean-Cryosphere-Atmosphere response (MOCA) [*Tarasov et al.*, 2012], and the Australian National University [ANU, *Lambeck et al.*, 2010] (see the supporting information for a description of the ice sheet reconstructions). In the ICE-5G and ICE-6G_A models, the topography with respect to LGM sea level includes the isostatic depression of the surface of the Earth due to the weight of the overlying ice. Each of the three representations of the LGM land ice distribution is equivalent to an approximately 120 m drop of eustatic sea level.

[7] The ICE-6G_A LGM reconstruction is a multidomed ice sheet with one maximum over Western Canada (the Keewatin Dome) and one dome southeast of James Bay, with both domes reaching up to 3000 m in height above LGM sea level (Figure 1a). The ICE-6G_A reconstruction has been reduced by ~1500 m in Central Canada and increased by less than 1000 m in both Western Canada and Northern Quebec and Labrador (Figure 1b) relative to ICE-5G. The changes between ICE-6G_A and the PMIP3-blended product are similar to the anomalies with respect to ICE-5G but of approximately half the magnitude (Figure 1c), a result that is based upon the fact that the PMIP3 reconstruction has apparently used ICE-6G as the primary component in producing the blended product over North America.

3. Results

3.1. Spin-Up to Equilibrium

[8] The initial LGM ICE-5G simulation and its corresponding preindustrial control simulation were each run for 3200 years (Figure 2). The perturbation LGM experiments (LGM ICE-6GA and LGM PMIP3) were then branched off the ICE-5G simulation at year 2000 and run for an additional 1200 years. The branch runs reach equilibrium within 700 years of the initial branch point. The LGM simulations have no residual temperature drift in the surface or deep oceans during equilibrium (see supporting information for details of the initial conditions for each run and control model drift).

[9] The initial LGM AMOC with ICE-5G boundary conditions (Figure 2a) requires approximately 1700 years of simulation to reach an equilibrium of approximately 10 Sv with a 2–3 Sv oscillation in the following 1000 years. The modern preindustrial climate, which exhibits a slight AMOC drift of about −4 Sv over 3000 years, is characterized by a magnitude of approximately 18 Sv near the end of our set of simulations, which is in good agreement with observations [*McCarthy et al.*, 2012] but with NADW not penetrating to sufficient depth [*Danabasoglu et al.*, 2012]. The AMOC in each of the three LGM experiments has an equilibrium strength which ranges between 10 and 11 Sv, which represents a reduction in strength of approximately 40% from modern. This AMOC reduction is in agreement with changes that are inferred to have occurred based upon Pa/Th proxy

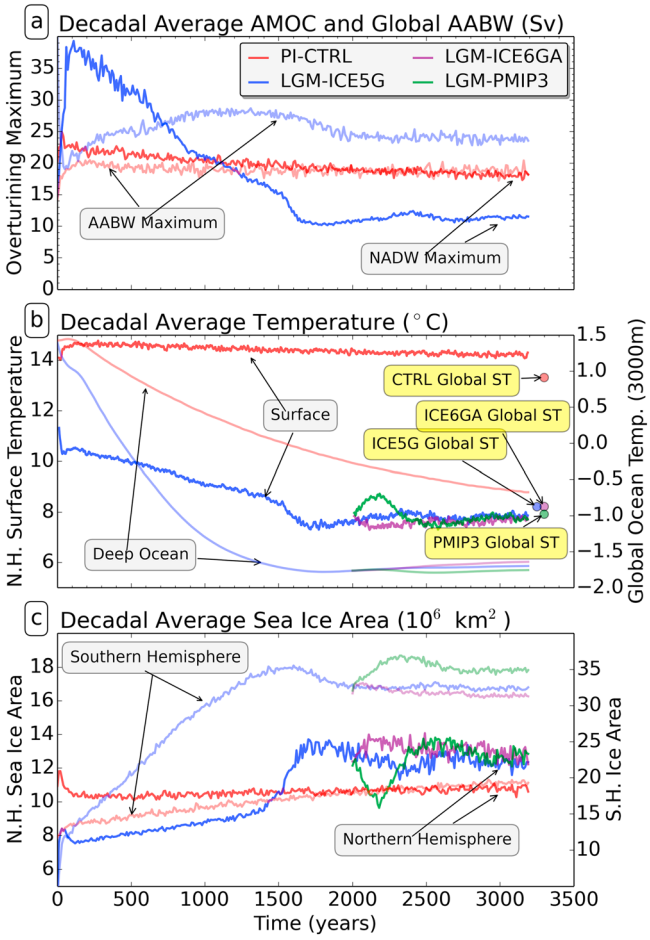

Figure 2. (a) Atlantic Meridional Overturning Circulation and Global Antarctic Bottom Water, (b) Northern Hemisphere surface temperature and globally averaged deep sea temperature at 3000 m, and (c) hemispheric sea ice area in the preindustrial control (red), ICE-5G (blue), ICE-6G_A (purple), and PMIP3 (green) LGM simulations. The global average surface temperature changes between the preindustrial control and LGM experiments are also highlighted in yellow in Figure 2b.

data in the Bermuda Rise region of the Atlantic [*McManus et al.*, 2004] and with a previous CSM1.4 LGM climate reconstruction [*Peltier and Solheim*, 2004]. These new results also agree with an earlier T42 resolution CCSM3 LGM simulation by *Otto-Bliesner et al.* [2006] but only when the original LGM T42 climate reconstruction was run to equilibrium with an additional 1400 years of simulation [*Brandefelt and Otto-Bliesner*, 2009]. PMIP2 LGM intercomparisons of AMOC strength, however, were not in general characterized by this strong reduction [*Otto-Bliesner et al.*, 2007]. It is therefore clearly important to assess whether the climate simulations have crossed the appropriate thresholds such as the thermal/sea ice threshold that we explicitly discuss below.

[10] In the original CCSM3 preindustrial control model, the Antarctic Bottom Water (AABW) cell is excessively strong (e.g., in the significantly improved CCSM4 PI control, the longitudinally averaged AABW overturning maximum in the circumpolar channel within which the Antarctic Circumpolar Current resides is only 8 Sv, which is near the lower end of available observations) [*Danabasoglu et al.*, 2012]. The global AABW cell is even stronger in our LGM simulation (22 to 24 Sv) as compared with the preindustrial control simulation (19 Sv) (Figure 2a). On this basis it is therefore clear that the CCSM3 results are liable to be erroneous in the Southern Hemisphere. The Northern Hemisphere mean annual surface temperature (Figure 2b) and Northern Hemisphere mean annual sea ice area (Figure 2c) are nevertheless well correlated with one another and with the Northern Hemisphere mean annual sea ice area and AMOC strength (Figure 2a). The three LGM simulations are 5.0°C to 5.3°C cooler than preindustrial in the global and annual means (Figure 2b), results that are also consistent with previous LGM studies [*Masson-Delmotte et al.*, 2006]. In spite of the radically different initial conditions employed in our analyses, the resulting LGM statistical equilibrium climate has therefore not been significantly affected. This is important and also clearly evident in the globally averaged deep ocean temperature at 3000 m (Figure 2b) which exhibits only minor variations in the LGM branch runs. The preindustrial control deep ocean temperature contains a long timescale drift and is cold compared with observations, whereas the LGM temperatures, which are near freezing, compare well with temperatures derived from pore fluid measurements [*Adkins et al.*, 2002].

[11] The preindustrial sea ice extent in CCSM3 does not drift significantly in the Northern Hemisphere and is consistent with the observed area of approximately 10 million km^2 [*Rayner et al.*, 2003]. However, the Southern Hemisphere sea ice extent is excessive in the preindustrial control and reaches approximately twice the observed area (Figure 2c) [see, e.g., *Holland and Raphael*, 2006]. In the Northern Hemisphere, each LGM experiment (including the "parent" ICE-5G simulation and the ICE-6G_A and PMIP3 branch runs) reaches an areal sea ice extent of approximately 13 million km^2, 2 million km^2 greater than present. The LGM Southern Hemisphere sea ice reaches an areal extent of 32–35 million km^2 and is excessive [see, e.g., *Waelbroeck et al.*, 2009] due to the biases in the control experiment. Of special interest in the spin-up to LGM equilibrium in the CCSM3 model is the transition to a North Atlantic characterized by significant winter sea ice in the North Atlantic subpolar gyre region over a period of a few decades between simulation years 1550 and 1650 in the ICE-5G simulation. The formation of this additional sea ice and accompanying AMOC reduction occurs once a nonlinear threshold is crossed, leading to a rapid increase of sea ice extent. The formation of this sea ice "lid," mainly in the January to April period, is a component of the extreme variability in the seasonal and interannual sea ice areal extent predicted by the model for the LGM North Atlantic in statistical equilibrium (Figure 2c) and clearly leads the reduction in AMOC by several decades. The large concentrations are also accompanied by increases in annual average sea ice thickness of 0.25 to 0.30 m over the North Atlantic subpolar gyre. This sea ice lid therefore plays a critical role in surface buoyancy forcing and the reorganization and reduction of the vigor of deep water formation sites (see Figure S2) during the transition period in which the nonlinear threshold is crossed.

3.2. Surface Response to Topographic Forcing

[12] The annual mean surface air temperature (SAT) anomalies between LGM ICE-6G_A and the preindustrial control are upward of 35°C colder at LGM over the center of the ice sheets at equilibrium. The SATs over the northern North Atlantic are 8–12°C colder over areas with new sea ice cover

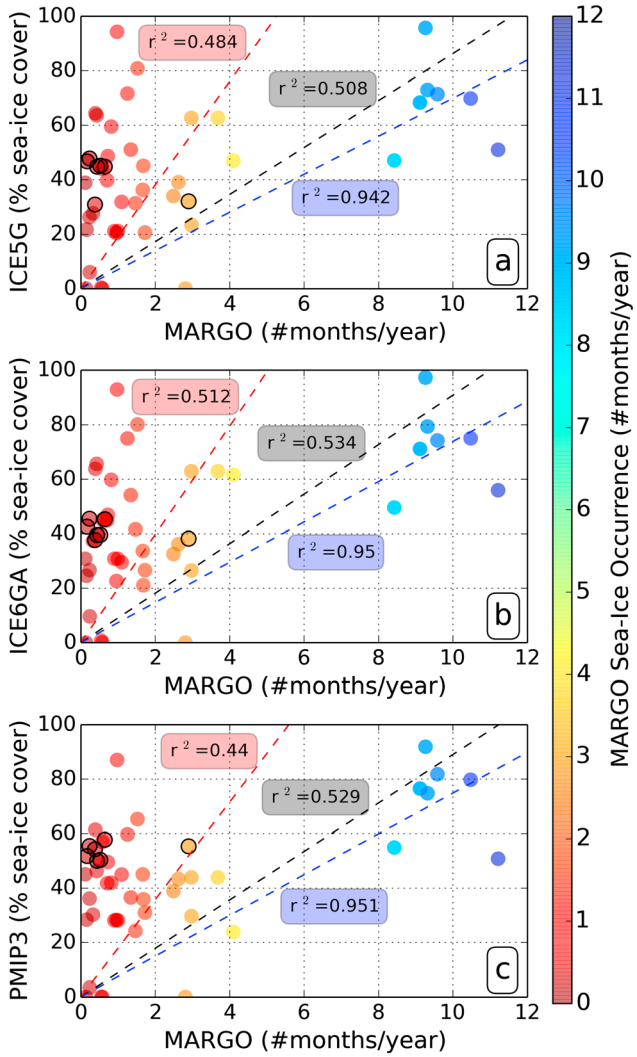

Figure 3. Scatterplots of reconstructed sea ice from MARGO in months of sea ice occurrence per year and the LGM mean annual sea ice concentration for (a) ICE5G, (b) ICE6G_A, and (c) PMIP3. R^2 correlations (observed versus model) are displayed for all data (black dashed line), data over the Davis Strait (blue dashed line), and data without the Davis Strait (red dashed line).

at LGM (Figure 1d). The SAT anomalies over the Laurentide Ice Sheet (Figures 1e and 1f) are consistent with the differences in ice sheet elevation, with anomalies that are 6–8°C warmer in the ICE-6G_A reconstruction. The warmer (cooler) areas in the surface air temperature anomalies correlate precisely with reductions (increases) in elevation differences between reconstructed ice heights in Figure 1. Also clearly evident is the downstream effect over the North Atlantic where the ICE-6G_A elevation differences are lower in the southern region of the Laurentide Ice Sheet and have significant influence over the subpolar gyre. The annual average temperature changes over the subpolar gyre are approximately 1 to 4°C warmer in the ICE-6G_A experiment as compared with the other two reconstructions, which are on the order of differences in the northern North Atlantic LGM versus modern Multiproxy Approach for the Reconstruction of the Glacial Ocean surface (MARGO) SST reconstructions [*Waelbroeck et al.*, 2009].

[13] The sea ice concentration anomalies between LGM ICE-6G_A and the preindustrial control show much of the northern North Atlantic covered with sea ice concentrations reaching 80% to 100% in March in sensitive deep water formation areas (e.g., the Norwegian Sea) where there was none present in the preindustrial control (Figures S1 and S2). The sea ice cap that forms in Boreal winter over the northern North Atlantic region is clearly visible in the sea ice anomaly differences between the three LGM experiments, with all three LGM experiments having a similar surface coverage but varying sea ice concentration and thickness. The ICE-6G_A sea ice is thinner in this region by up to 30 cm as compared with the PMIP3 experiment but less so as compared with the ICE-5G experiment (Figure S1). A thickening in sea ice around the subpolar gyre with respect to the ICE-6G_A simulation is postulated to be a consequence of changes in wind stress forcing (Figure S2). In the LGM experiments, the zonal winds over the North Atlantic shift southward and would thus impact sea ice drift to more southerly latitudes. These changes have direct implications for the stability of the AMOC in this region, especially if the AMOC strength is near a critical threshold [e.g., *Oka et al.*, 2012]. The changes in convection indicated by the anomalies in mixed layer depth (Figure S2) also demonstrate that while some convective regions cease to exist in the reduced AMOC mode, convection strengthens in other regions (e.g., south of Greenland). Therefore, the ice sheet reconstruction appears to influence the formation of Glacial North Atlantic Intermediate Water (GNAIW) in the subpolar region [*Duplessy et al.*, 1988] rather than the overall zonally averaged mass transport stream function in the North Atlantic.

3.3. Sea Ice Proxy Data and Model Comparison

[14] The MARGO initiative [*Waelbroeck et al.*, 2009] provides sea ice proxy data mainly inferred from dinocysts. Monthly sea ice occurrence data indicate the number of months that sea ice is present at a particular core location based upon the transfer function inferred on the basis of modern core top observations. Model-model intercomparisons of sea ice in the North Atlantic region (PMIP1/PMIP2) reveal large differences in the southerly extent of modeled sea ice [cf. *Kageyama et al.*, 2006, Figure 5]. Figures 3a–3c show scatter correlation plots of the model mean annual sea ice concentration versus sea ice occurrence data at the location of the MARGO sites in the North Atlantic and the r^2 (goodness of fit) statistic (Figure S3). The main feature of the MARGO data is that there is suggested to be little (but nonzero) sea ice throughout the year in the Labrador and Irminger Sea regions (the subpolar gyre) except at one location (data points highlighted in black). This is in sharp contrast to the results obtained in the LGM simulations for this region. The model-data correlation, however, is very high ($r^2 = 0.95$) over the Davis Strait between Greenland and Baffin Island. Of interest is the strong sea ice tongue that extends from the tip of exposed LGM land off the coast of Newfoundland and farther into the northeastern North Atlantic in each of the simulations (see Figure S2). Unfortunately, there is an absence of sea ice proxy data in this southern subpolar gyre region to compare with the large-modeled concentrations that are predicted. The model fits to the MARGO data are moderate with an r^2 of approximately 0.5 in each simulation, demonstrating the spread of the results and the (apparently) somewhat excessive sea ice simulated in the model as compared with proxy data-based inferences.

4. Concluding Remarks

[15] The three LGM experiments we have described are all consistent with proxy data that indicate that the LGM climate regime was characterized by a sluggish, less well ventilated North Atlantic Ocean circulation [e.g., *McManus et al*., 2004]. We suggest that the primary cause of this reduction in AMOC strength is the formation of a sea ice cap in the Labrador and Irminger Seas in the North Atlantic subpolar gyre region. In our mini-ensemble of analyses based upon the implementation of different continental ice sheet reconstructions, this forms after approximately 1500 years of simulation in the ICE-5G "parent" experiment. We have shown that the magnitude of downstream effects play a significant role in the formation of the sea ice cap in the North Atlantic and significantly control the locations of GNAIW and GNADW formation. The modification of activity in the critical deep water formation site in the Labrador Sea and the cessation of activity in the Norwegian Sea result in an LGM AMOC strength reduced by approximately 40% from modern. Our results nevertheless imply that each of the ice sheet reconstructions produce little difference in the zonally averaged mass stream function in the glacial North Atlantic and the influence of each is sufficient to maintain the reduced strength of the AMOC at LGM in this particular model, in agreement with the proxy-inferred strength.

[16] The MARGO data do suggest the presence of sea ice in the North Atlantic subpolar gyre region but not for the same monthly duration inferred. However, winter conditions are most important for the formation of NADW and both our model simulations and proxy data suggest large variability of northern North Atlantic sea ice during its annual cycle (see the animation provided in the supporting information). Such large-amplitude variations in sea surface conditions might well explain the difficulties that have been experienced in obtaining agreement between paleoceanographic proxy-based inferences and model predictions given that conditions were not analogous to modern. This could also explain discrepancies between inferences based upon the use of different proxies which are characterized by moderate to low reliability due also to low dinocyst concentrations which reflect low productivity [*de Vernal et al*., 2005]. The few high-resolution records available for the LGM time slice do indeed indicate very large amplitude variations of sea ice [*de Vernal et al*., 2000, 2006]. A highly dynamical ocean, characterized by instability of sea surface conditions and large-amplitude variations of sea ice cover on both interannual and decadal time scales is inferred to be a consistent feature of the data.

[17] **Acknowledgments.** Anne de Vernal has provided helpful discussions of the sea ice proxy data. Our climate simulations were performed on the University of Toronto SciNet facility, a component of the Compute Canada HPC platform. The research of WRP at Toronto is supported by NSERC Discovery grant A9627.

[18] The Editor thanks an anonymous reviewer for his assistance in evaluating this paper.

References

Adkins, J. F., K. McIntyre, and D. P. Schrag (2002), The salinity, temperature, and $\delta^{18}O$ of the glacial deep ocean, *Science*, *298*(5599), 1769–1773, doi:10.1126/science.1076252.

Argus, D. F., and W. R. Peltier (2010), Constraining models of postglacial rebound using space geodesy: A detailed assessment of model ICE-5G (VM2) and its relatives, *Geophys. J. Int.*, *181*, 697–723, doi:10.1111/j.1365-246X.2010.04562.x.

Boyle, E., and H. Leach (1995), Last-Glacial-Maximum North Atlantic Deep Water: On, off or somewhere in-between?, *Philos. Trans. R. Soc. B*, *348*, 243–253, doi:10.1098/rstb.1995.0066.

Brady, E. C., B. L. Otto-Bliesner, J. E. Kay, and N. Rosenbloom (2013), Sensitivity to glacial forcing in the CCSM4, *J. Clim.*, *26*, 1901–1925, doi:10.1175/JCLI-D-11-00416.1.

Brandefelt, J., and B. L. Otto-Bliesner (2009), Equilibration and variability in a Last Glacial Maximum climate simulation with CCSM3, *Geophys. Res. Lett.*, *36*, L19712, doi:10.1029/2009GL040364.

Collins, W. D., et al. (2006), The Community Climate System Model: CCSM3, *J. Clim.*, *19*, 2122–2143.

Danabasoglu, G., S. C. Bates, B. P. Briegleb, S. R. Jayne, M. Jochum, W. G. Large, S. Peacock, and S. G. Yeager (2012), The CCSM4 ocean component, *J. Clim.*, *25*, 1361–1389, doi:10.1175/JCLI-D-11-00091.1.

de Vernal, A., C. Hillaire-Marcel, J. Turon, and J. Matthiessen (2000), Reconstruction of sea-surface temperature, salinity, and sea-ice cover in the northern North Atlantic during the Last Glacial Maximum based on dinocyst assemblages, *Can. J. Earth Sci.*, *37*, 725–750.

de Vernal, A., et al. (2005), Reconstruction of sea-surface conditions at middle to high latitudes of the Northern Hemisphere during the Last Glacial Maximum (LGM) based on dinoflagellate cyst assemblages, *Quat. Sci. Rev.*, *24*, 897–924.

de Vernal, A., A. Rosell-Mele, M. Kucera, C. Hillaire-Marcel, F. Eynaud, M. Weinelt, T. Dokken, and M. Kageyamag (2006), Comparing proxies for the reconstruction of LGM sea-surface conditions in the northern North Atlantic, *Quat. Sci. Rev.*, *26*, 2820–2834.

Duplessy, J. C., N. J. Shackleton, R. G. Fairbanks, L. Labeyrie, D. Oppo, and N. Kallel (1988), Deepwater source variations during the last climate cycle and their impact on the global deepwater circulation, *Paleoceanography*, *3*(3), 343–360, doi:10.1029/PA003i003p00343.

Holland, M. M., and M. N. Raphael (2006), Twentieth century simulation of the Southern Hemisphere climate in coupled models. Part II: Sea ice conditions and variability, *Clim. Dyn.*, *26*, 229–245.

Kageyama, M., et al. (2006), Last Glacial Maximum temperatures over the North Atlantic, Europe and Western Siberia: A comparison between PMIP models, MARGO sea surface temperatures and pollen-based reconstructions, *Quat. Sci. Rev.*, *25*, 2082–2102.

Kageyama, M., et al. (2013), Climatic impacts of fresh water hosing under Last Glacial Maximum conditions: A multi-model study, *Clim. Past*, *9*, 935–953.

Lambeck, K., A. Purcell, J. Zhao, and N.-O. Svensson (2010), The Scandinavian Ice Sheet: From MIS 4 to the end of the Last Glacial Maximum, *Boreas*, *39*(2), 410–435, doi:10.1111/j.1502-3885.2010.00140.x.

Lynch-Stieglitz, J., et al. (2007), Atlantic meridional overturning circulation during the Last Glacial Maximum, *Science*, *316*, 66–69, doi:10.1126/science.1137127.

Mashayek, A., R. Ferrari, G. Vettoretti, and W. R. Peltier (2013), The role of geothermal heat flux in driving the abyssal ocean circulation, *Geophys. Res. Lett.*, *40*, 3144–3149, doi:10.1002/grl.50640.

Masson-Delmotte, V., et al. (2006), Past and future polar amplification of climate change: Climate model intercomparisons and ice-core constraints, *Clim. Dyn.*, *26*, 513–529, doi:10.1007/s00382-005-0081-9.

McCarthy, G. D., E. Frajka-Williams, W. E. Johns, M. O. Baringer, C. S. Meinen, H. L. Bryden, D. Rayner, A. Duchez, C. D. Roberts, and S. A. Cunningham (2012), Observed interannual variability of the Atlantic meridional overturning circulation at 26.5°N, *Geophys. Res. Lett.*, *39*, L19609, doi:10.1029/2012GL052933.

McManus, J. F., R. Francois, J.-M. Gherardi, L. D. Keigwin, and S. Brown-Leger (2004), Collapse and rapid resumption of Atlantic meridional circulation linked to deglacial climate changes, *Nature*, *428*, 834–837, doi:10.1038/nature02494.

Oka, A., H. Hasumi, and A. Abe-Ouchi (2012), The thermal threshold of the Atlantic meridional overturning circulation and its control by wind stress forcing during glacial climate, *Geophys. Res. Lett.*, *39*, L09709, doi:10.1029/2012GL051421.

Oppo, D. W., and W. B. Curry (2012), Deep Atlantic Circulation during the Last Glacial Maximum and deglaciation, *Nat. Educ. Knowl.*, *3*(10), 1.

Otto-Bliesner, B. L., E. C. Brady, G. Clauzet, R. Tomas, S. Levis, and Z. Kothalava (2006), Last Glacial Maximum and Holocene climate in CCSM3, *J. Clim.*, *19*, 2526–2544.

Otto-Bliesner, B. L., C. D. Hewitt, T. M. Marchitto, E. Brady, A. Abe-Ouchi, M. Crucifix, S. Murakami, and S. L. Weber (2007), Last Glacial Maximum ocean thermohaline circulation: PMIP2 model intercomparisons and data constraints, *Geophys. Res. Lett.*, *34*, L12706, doi:10.1029/2007GL029475.

Peltier, W. R. (1994), Ice age paleotopography, *Science*, *265*, 195–201.

Peltier, W. R. (2004), Global glacial isostasy and the surface of the ice-age Earth: The ICE-5G (VM2) model and GRACE, *Annu. Rev. Earth Planet. Sci.*, *32*, 111–149.

Peltier, W. R., and R. G. Fairbanks (2006), Global glacial ice volume and Last Glacial Maximum duration from an extended Barbados sea level record, *Quat. Sci. Rev.*, *25*, 3322–3337.

Peltier, W. R., and L. P. Solheim (2004), The climate of the Earth at Last Glacial Maximum: Statistical equilibrium state and a mode of internal variability, *Quat. Sci. Rev.*, *23*, 335–357.

Radi, T., and A. de Vernal (2008), Last glacial maximum (LGM) primary productivity in the northern North Atlantic Ocean, *Can. J. Earth Sci.*, *45*, 1299–1316.

Rayner, N. A., D. E. Parker, E. B. Horton, C. K. Folland, L. V. Alexander, D. P. Rowell, E. C. Kent, and A. Kaplan (2003), Global analyses of sea surface temperature, sea ice, and night marine air temperature since the late nineteenth century, *J. Geophys. Res.*, *108*(14), 4407, 10.1029/2002JD002670.

Tarasov, L., A. S. Dyke, R. M. Neal, and W. R. Peltier (2012), A data-calibrated distribution of deglacial chronologies for the North American ice complex from glaciological modelling, *Earth Planet. Sci. Lett.*, *315-316*, 30–40, doi:10.1016/j.epsl.2011.09.010.

Waelbroeck, C., et al. (2009), Constraints on the magnitude and patterns of ocean cooling at the Last Glacial Maximum, *Nat. Geosci.*, doi:10.1038/NGEO411.

Weber, S. L., S. S. Drijfhout, A. Abe-Ouchi, M. Crucifix, M. Eby, A. Ganopolski, S. Murakami, B. Otto-Bliesner, and W. R. Peltier (2007), The modern and glacial overturning circulation in the Atlantic ocean in PMIP coupled model simulations, *Clim. Past*, *3*, 51–64, doi:10.5194/cp-3-51-2007.